Electronic supplementary information

Counter Ion-Regulated Heterostructured Co@Fe-Based Core@Shell Materials: As Remarkable Bifunctional Electrodes for Green H_2 Production

Gaddam Rajeshkhanna,*[a] Apurba Borah,[a] Thangjam Ibomcha Singh,[b] Thanh Hai Nguyen,[c] Van An Dinh,[d] Nam Hoon Kim,[c]* Joong Hee Lee*[ce]

[a]*Department of Chemistry, National Institute of Technology Warangal, Warangal 506004 Telangana, India, E-mail: grkhanna@nitw.ac.in*
[b]*Department of Physics, Manipur University, Canchipur, Manipur, 795003, India*
[c]*Department of Nano Convergence Engineering, Jeonbuk National University, Jeonju, Jeonbuk, 54896, Republic of Korea. E-mail: nhk@jbnu.ac.kr; jhl@jbnu.ac.kr*
[d]*Department of Precision Engineering, Graduate School of Engineering, Osaka University, 2-1, Yamada-oka, Suita, Osaka 565-0871, Japan*
[e]*Center for Carbon Composite Materials, Department of Polymer-Nano Science and Technology, Jeonbuk National University, Jeonju, Jeonbuk, 54896, Republic of Korea*

1. Experimental section

1.1. Synthesis of core-shell type $Co(OH)_2$@FeOOH/NF, Co_3O_4@Fe_3O_4/NF, and Co_2P@Fe_2P/NF

A core-shell structure of $Co(OH)_2$@FeOOH on Ni-foam (NF) was successfully synthesized through a two-step hydrothermal route. In the initial step, $Co(OH)_2$/NF was prepared using a straightforward hydrothermal method. Specifically, 1 mmol of $Co(NO_3)_2.6H_2O$ (99.99%, Sigma-Aldrich), 2 mmol of NH_4F (99.99%, Sigma-Aldrich), and 2 mmol of $CO(NH_2)_2$ (>99.5%, Sigma-Aldrich) were dissolved in 50 mL of deionized water (DI) with vigorous stirring at room temperature for 30 minutes. The resulting solution was transferred into a 70 mL Teflon-lined stainless-steel autoclave. A piece of Ni-foam (2 × 4 cm^2) was pre-treated by cleaning in 3 M HCl to eliminate the surface oxide layer, followed by ultrasonic cleaning in DI water for 15 minutes on several times. Subsequently, the pre-cleaned Ni-foam was immersed in the solution, supported against the Teflon cup, sealed, and heated at 120 °C for 8 hours. The resulting $Co(OH)_2$/NF precursor was rinsed with DI water and ethanol, then dried overnight at 60 °C. In the second hydrothermal step, a solution containing 0.5 mmol of $Fe(NO_3)_3.9H_2O$, 1

mmol of NH_4F, and 1 mmol of $CO(NH_2)_2$ in 50 mL of DI water was stirred for approximately 10 minutes for homogeneity. This solution was added to a 70 mL Teflon cup. The previously prepared $Co(OH)_2$/NF was introduced into this solution, and the sealed system was heated at 120 °C for 8 hours. The resulting sample ($Co(OH)_2$@FeOOH/NF) was washed with DI water and ethanol, then dried at 60 °C overnight. The Co_3O_4@Fe_3O_4/NF sample was obtained by subjecting the $Co(OH)_2$@FeOOH/NF sample to oxidation through heat treatment in a tubular furnace at 300 °C under an air atmosphere for 2 hours. To produce the Co_2P@Fe_2P/NF sample, the $Co(OH)_2$@FeOOH/NF sample and sodium hypophosphite ($Na_2H_2PO_4.2H_2O$) were placed in a tubular furnace, with $Na_2H_2PO_4.2H_2O$ positioned upstream of the furnace, and heated at 350 °C under an argon atmosphere for 3 hours. For comparison, $Co(OH)_2$ and FeOOH materials were separately synthesized using the same concentrations and hydrothermal conditions.

1.2. Characterization

The synthesized materials were subjected to comprehensive characterization to assess their structure and phase. Powder X-ray diffraction (PXRD) was performed using a Rigaku Corporation instrument in Japan, employing CuKα radiation with a wavelength (λ) of 0.154 nm. This technique provided insights into the structure and phase of the materials. For a detailed examination of surface morphological features and elemental distribution, field-emission scanning electron microscopy (FE-SEM) was employed, utilizing a JSM-6701F instrument from JEOL in Japan. Additionally, the core-shell structure, crystallinity, and elemental composition were scrutinized using high-resolution transmission electron microscopy (HR-TEM), scanning transmission electron microscopy (STEM), and energy-dispersive X-ray spectroscopy (EDX) on a JEM-2200 FS instrument by JEOL Ltd. operating at 200 kV. To further analyze the surface elemental compositions and valence states, X-ray photoelectron spectroscopy (XPS) was conducted using a Theta Probe instrument from Thermo

Fisher Scientific in the UK. This technique provided valuable information about the chemical states of elements on the material's surface. In summary, the combination of these advanced characterization techniques enabled a comprehensive understanding of the structural, morphological, and compositional aspects of the synthesized materials.

1.3. Fabrication of electrodes and electrochemical measurements

The electrochemical performances of the in situ grown materials on Ni foam were assessed using a CHI 660E electrochemical workstation. In the standard three-electrode evaluation setup, binder-free $Co(OH)_2$@FeOOH/NF, Co_3O_4@Fe_3O_4/NF, and Co_2P@Fe_2P/NF served as the working electrode (with a 1 cm^2 area), an Hg/HgO electrode functioned as the reference electrode, and a graphite rod acted as the counter electrode. As a point of reference, the as-synthesized $Co(OH)_2$/NF (core) and FeOOH/NF (shell) were directly employed as working electrodes. For the fabrication of the alkaline electrolysis cell, the working electrodes were utilized as both the anode and cathode. The electrocatalytic activities of synthesized electrode materials were compared with the state-of-the-art catalysts, commercial Pt/C (20 wt.%) and RuO_2 (99.9 wt.%) catalyst inks were prepared separately by dispersing 5 mg of each sample in a solution mixture comprising 750 µL of isopropyl alcohol, 200 µL of deionized (DI) water, and 50 µL of 5% Nafion. This mixture underwent ultrasonication treatment for about 45 minutes and was then coated onto a 1 cm^2 area of Ni foam.

In three electrode tests, all potentials were referenced to reversible hydrogen electrode (RHE) potentials, derived from Hg/HgO electrode potentials using the Nernst equation: $E_{RHE} = E_{Ag/AgCl} + 0.059 \times pH + 0.098\,V$. To ensure the accuracy, all RHE potentials were iR-corrected using the equation: $E_{corr} = E_{mea} - iR$, where E_{corr} is the iR-corrected potential, E_{mea} is the experimentally measured potential, i is the current and R is the uncompensated ohmic electrolyte resistance measured by electrochemical impedance spectroscopy (EIS) at high frequency. The overpotential (η) values were evaluated from an equation of

$\eta = E_{RHE} - 1.23\ V$. The Tafel slopes were obtained from LSV curves using the following equation $\eta = b\ log(j) + a$, where η is overpotential, b is Tafel slope, j is current density.

1.4. Density functional theory calculation methods

All the spin-polarized density functional theory (DFT) calculations were performed using Vienna Ab Initio Package (VASP).[1-2] The exchange-correlation interaction was described using generalized gradient approximation (GGA) parameterized by the Perdew-Burke-Enzerhof.[3] A cut-off energy of 500 eV was used together with the projected augmented wave (PAW) potentials.[4] Grimme D3 correction was used to satisfy the dispersion interactions.[5] A vacuum spacing of 15 Å was added into the z-direction to avoid the interaction between repeated slabs. A Γ-centered k-point of 3×3×1 was used in this study. A geometry optimization was allowed to relax until the residual force change was less than 0.03 eV $Å^{-1}$.

The Gibbs free energy was calculated as follows:

$$\Delta G = \Delta E_{ads} + \Delta E_{ZPE} - T\Delta S$$

where ΔE_{ads} is the adsorption energy of intermediates. ΔE_{ZPE} and ΔS are changes in zero-point energy and entropy between adsorbed intermediates and molecule in gas phase, respectively. T is temperature (K).

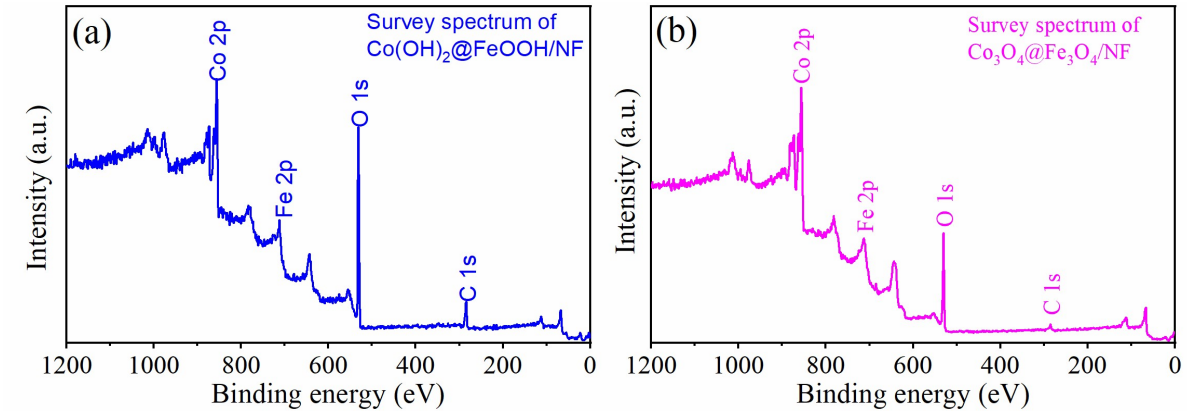

Fig. S1 XPS survey spectrum of (a) $Co(OH)_2$@FeOOH/NF, and (b) Co_3O_4@Fe_3O_4/NF.

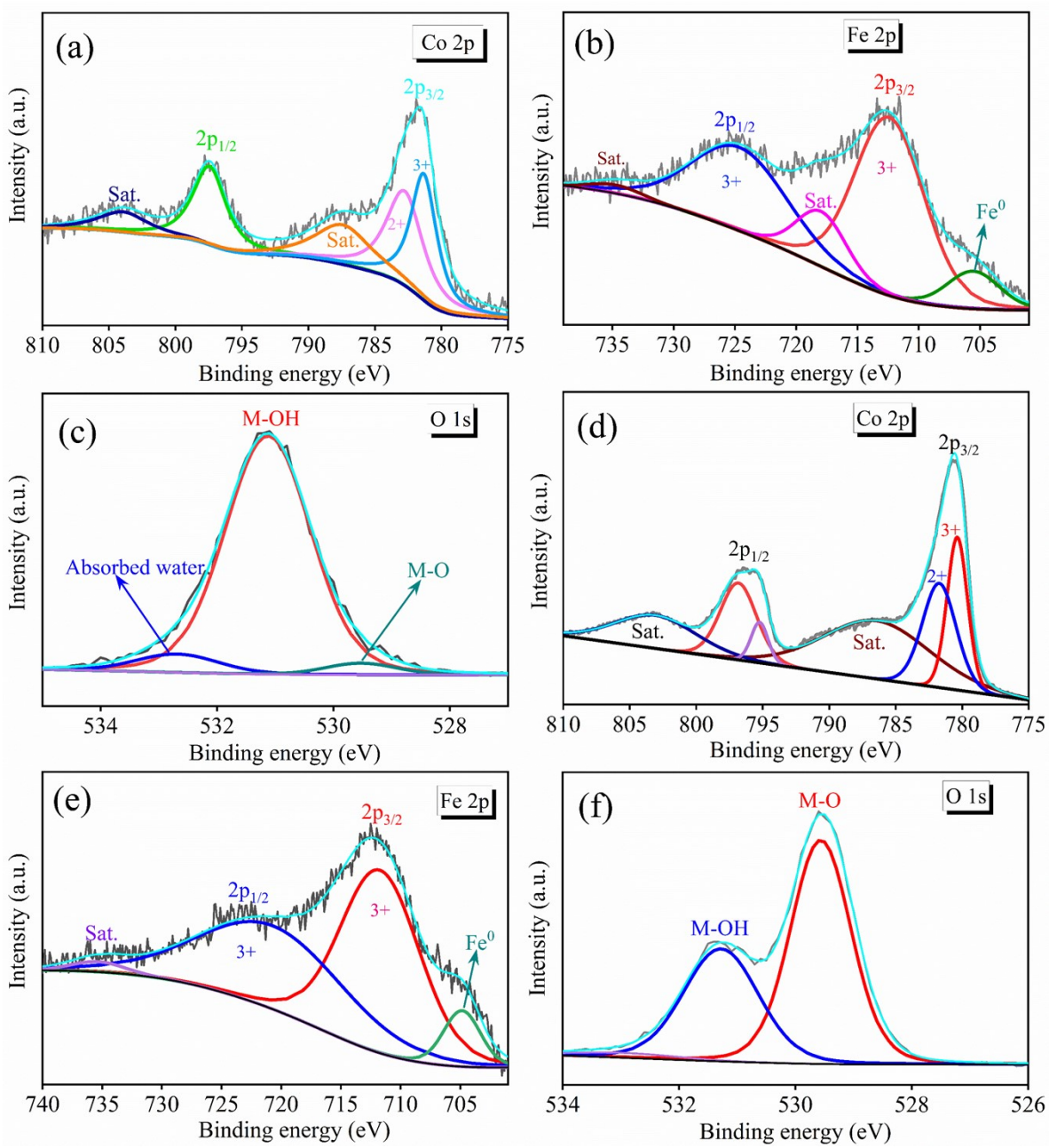

Fig. S2 XPS deconvoluted spectra for (a) Co 2p, (b) Fe 2P, (c) O 1s of $Co(OH)_2$@FeOOH/NF, and (d) Co 2p, (e) Fe 2p, (f) O 1s of Co_3O_4@Fe_3O_4/NF.

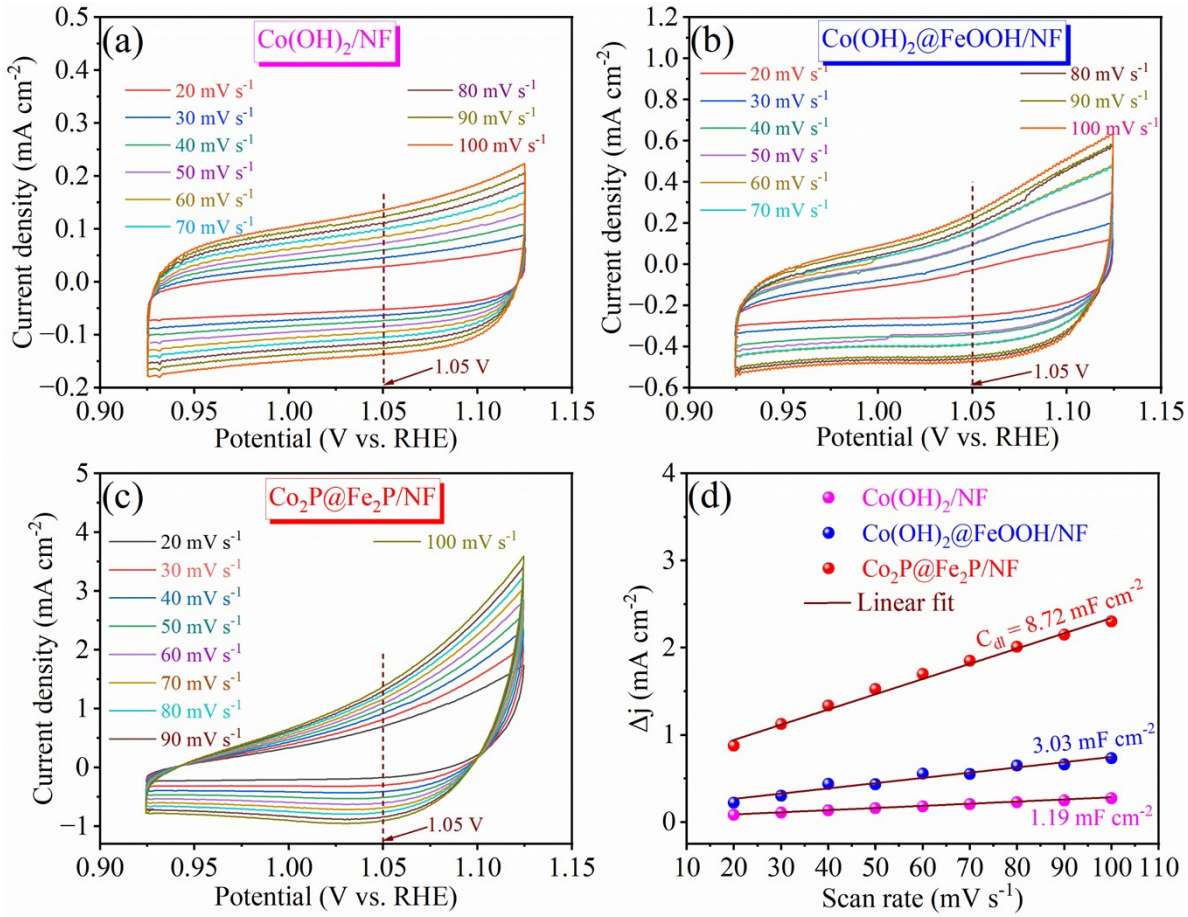

Fir. S3 Cyclic voltammograms at different scan rates of (a) $Co(OH)_2$/NF, (b) $Co(OH)_2$@FeOOH/NF, (c) Co_2P@Fe_2P/NF, and (d) scan rate vs. difference in anodic and cathodic current densities (Δj) plot at 1.05 V with C_{dl} values.

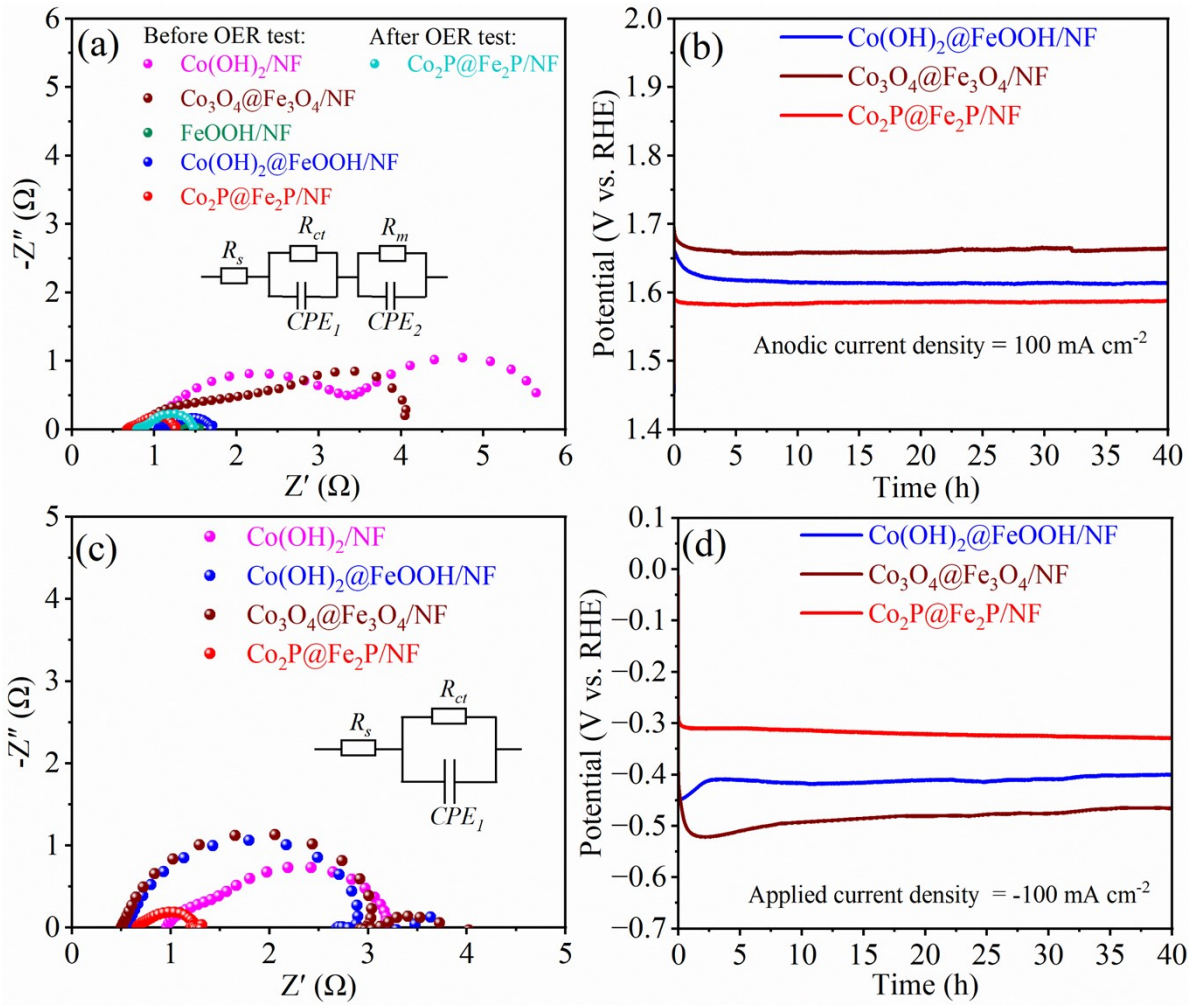

Fig. S4 (a) Nyquist plots in OER region at 1.53 V, (b) chronopotentiometric stability tests for OER at 100 mA cm^{-2} current density, (c) Nyquist plots before HER test at -0.275 V, and (d) chronopotentiometric stability tests for HER at -100 mA cm^{-2} current density.

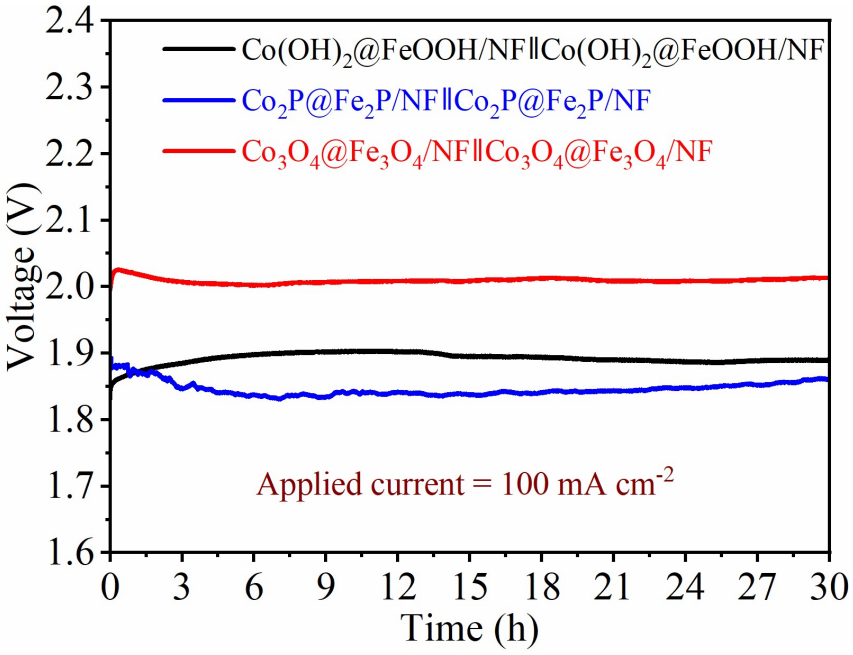

Fig. S5 Chronopotentiometric stability test of fabricated electrolyzers at 100 mA cm^{-2}.

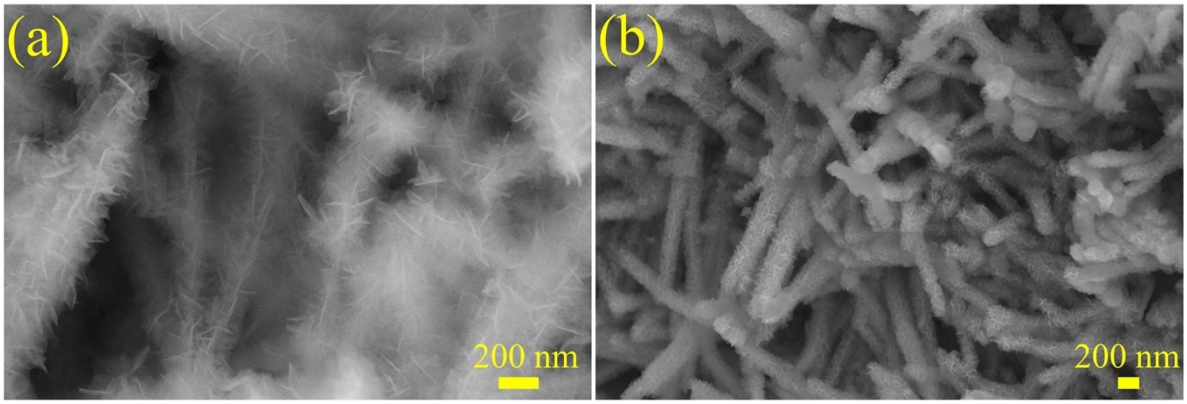

Fig. S6 Potst-OER FESEM images of (a) $Co(OH)_2$@FeOOH, and (b) Co_2P@Fe_2P.

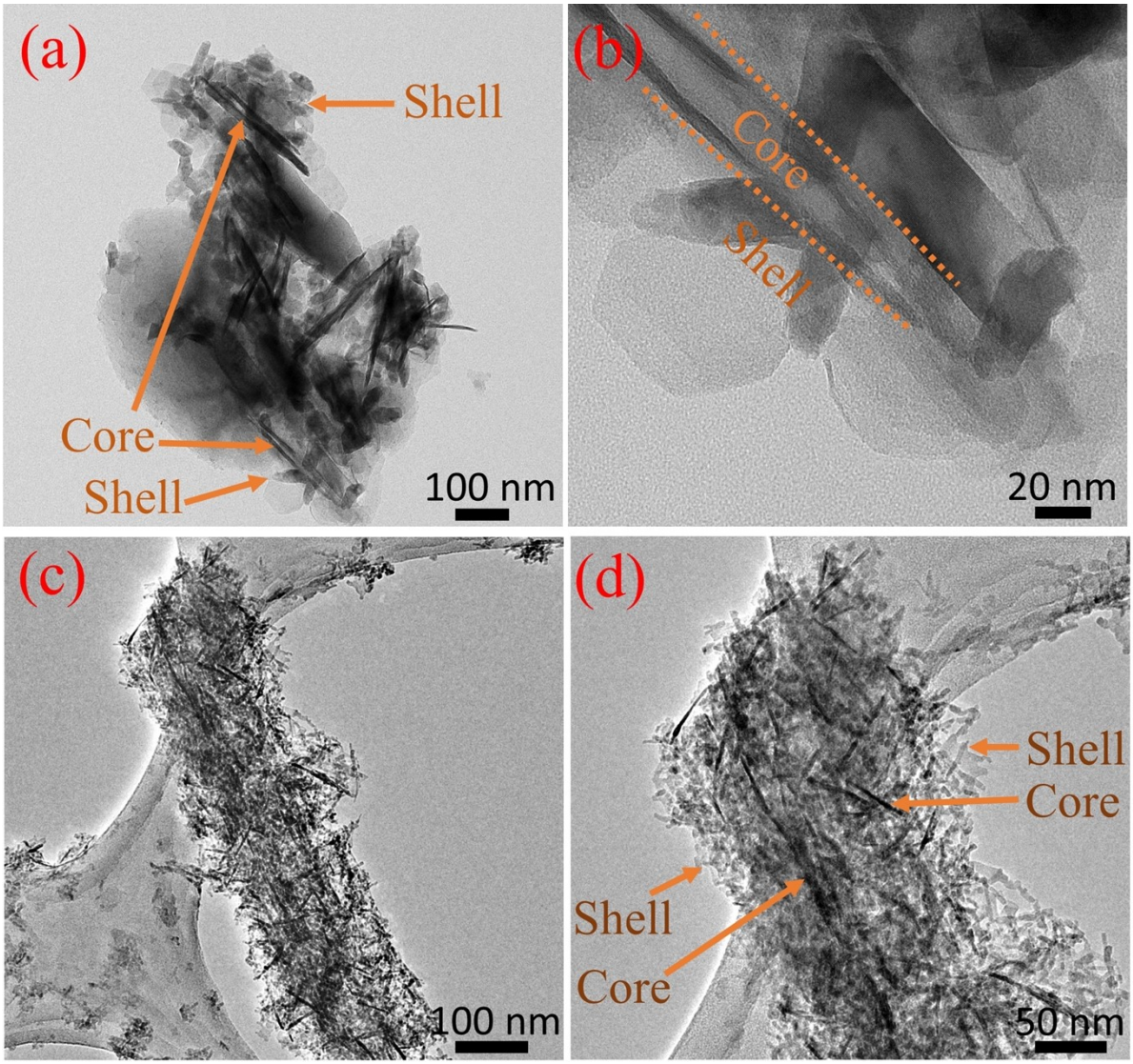

Fig. S7 Post-OER TEM images of (a,b) $Co(OH)_2$@FeOOH, (c,d) Co_2P@Fe_2P.

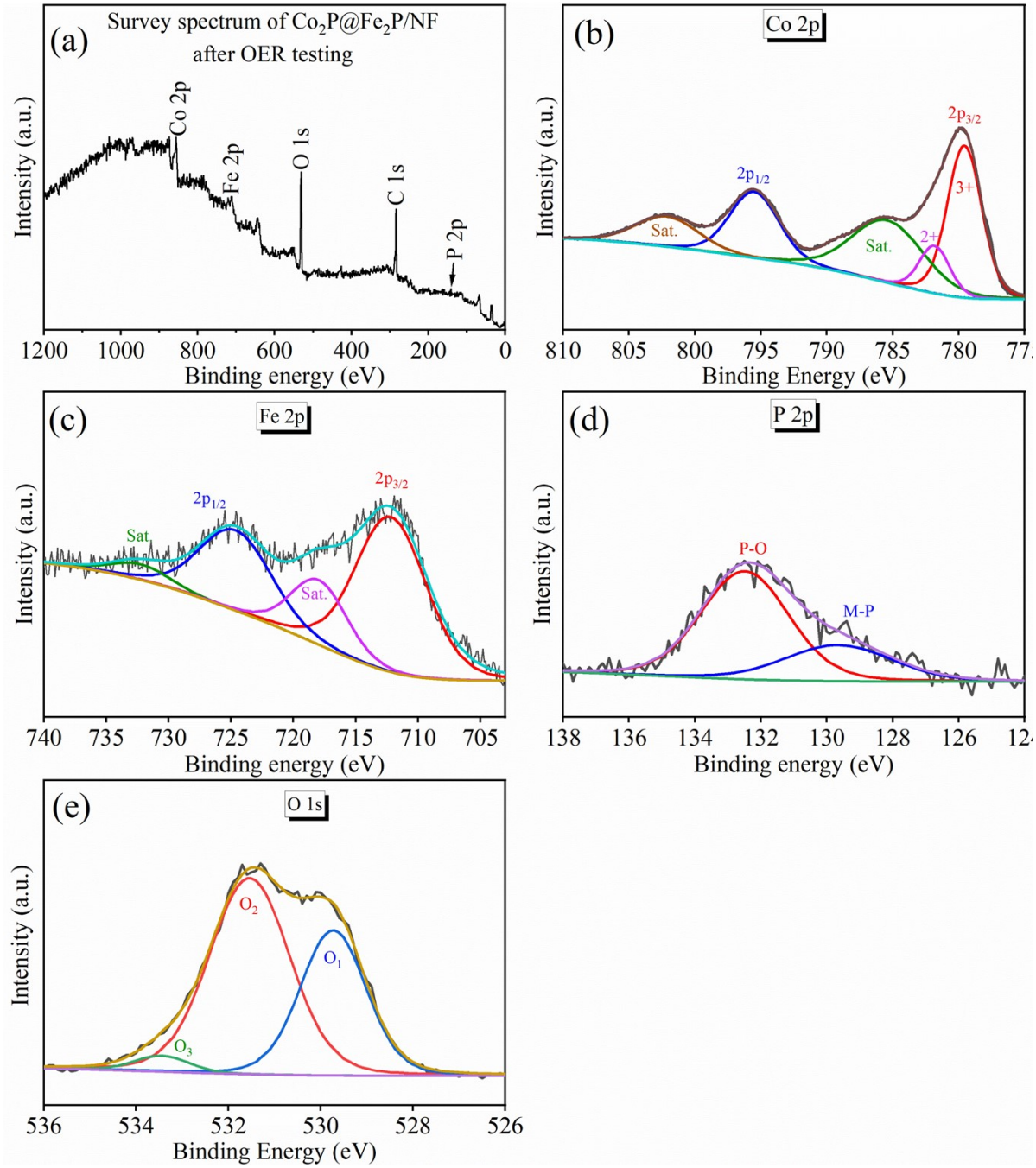

Fig. S8 XPS (a) survey spectrum, deconvoluted spectra for (b) Co 2p, (c) Fe 2p, (d) P 2p, and (e) O 1s of $Co_2P@Fe_2P$/NF after OER testing.

Table S1. Comparison of OER performance of the synthesized electrode materials with the results of recently reported non-noble transition metal-based electrocatalysts.

Sl. No.	Electrode material	Electrolyte	$\eta_{10}{}^{a)}$ (mV)	$\eta_{50}{}^{b)}$ (mV)	Tafel slope (mV dec^{-1})	Reference
1	$Co(OH)_2$@FeOOH /NF	1 M KOH	-	237	34[c)]	This work
2	Co_3O_4@Fe_3O_4/NF	1 M KOH	-	378	70[c)]	This work
3	Co_2P@Fe_2P/NF	1 M KOH	-	267	65[c)]	This work
4	$Zn_{1-x}Fe_x$-LDH/Ni-foam	1 M KOH	-	288	58	S6
5	$Zn_{1-x}Fe_x$-oxyselenide/Ni-foam	1 M KOH	-	277	54	S7
6	$Co_{0.025}$-NiFe-LDH/NF	1 M KOH	208	-	50.9	S8
7	Co(OH)F@CoFe-LDH	1 M KOH	240	-	25.4	S8
8	Co_3Fe_7@NCNTFs	1 M KOH	264	-	79	S9
9	CoFeSP/CNT	1 M KOH	262	-	54	S10
10	$CoMoRuO_x$-350	1 M KOH	250	-	83.8	S11
11	Mo-CoP (1/2.3)	1 M KOH	317	-	82	S12
12	Co_3S_4@MoS_2-Ni_3S_2	1 M KOH	-	270	69	S13
13	Co_3S_4@rGO	0.5 M H_2SO_4	350	-	65	S14
14	Co_3O_4@rGO	0.5 M H_2SO_4	380	-	121	S14
15	FeCoNiP@NC	1 M KOH	266	-	35.6	S15
16	Co-Fe oxyphosphide	1 M KOH	280	-	53	S16
17	Co@BNPCFs-800	1 M KOH	324	-	55.6	S17
18	Co/Mo_2C@C	1 M KOH	254	-	136	S18
19	Ni-Fe-S/Cu	1 M KOH	375.3	450	79.5	S19
20	Co@NC nanocage/HCF_{200}	O_2 sat. 1 M KOH	396	-	90.22	S20

[a)] η_{10} is overpotential at a current density of 10 mA cm^{-2}; [b)] $\eta_{50}$is overpotential at a current density of 50 mA cm^{-2}; [c)] Tafel slope at low overpotential region.

Table S2. Comparison of HER performance of the synthesized electrode materials with recently reported non-noble transition metal-based results.

Sl. No.	Electrode material	Electrolyte	η_{-10} [a)] (mV)	η_{-50} [b)] (mV)	Tafel slope (mV dec^{-1})	Reference
1	$Co(OH)_2$@FeOOH /NF	1 M KOH	175	275	140	This work
2	Co_3O_4@Fe_3O_4/NF	1 M KOH	255	352	135	This work
3	Co_2P@Fe_2P/NF	1 M KOH	95	196	120	This work
4	$Zn_{1-x}Fe_x$-LDH/Ni-foam	1 M KOH	221	327	150	S6
5	$Zn_{1-x}Fe_x$-oxyselenide/Ni-foam	1 M KOH	238	347	153	S6
6	$Co_{0.025}$-NiFe-LDH/NF	1 M KOH	113	-	114.5	S7
7	Co(OH)F@CoFe-LDH	1 M KOH	130	-	82.9	S8
8	Co3Fe7@NCNTFs	1 M KOH	197	-	62	S9
9	CoFeSP/CNT	1 M KOH	130	-	70	S10
10	Mo-CoP (1/2.3)	1 M KOH	118	-	76	S12
11	Mo-CoP (1/2.3)	0.5 M H_2SO_4	116		69	S12
12	Co_3S_4@MoS_2-Ni_3S_2	1 M KOH	136	-	72	S13
13	Co_3S_4@rGO	0.5 M H_2SO_4	151	-	59	S14
14	Co_3O_4@rGO	0.5 M H_2SO_4	234	-	153	S14
15	FeCoNiP@NC	1 M KOH	187	-	51.7	S15
16	Co-Fe oxyphosphide	1 M KOH	180	-	62	S16
17	Co@BNPCFs-800	1 M KOH	151.3		91.78	S17
18	Co/Mo_2C@C	1 M KOH	98	-	68	S18
19	Co@NC nanocage/HCF_{200}	N_2 sat. 1 M KOH	261.4	-	109.88	S20
20	Fe-Ni_5P_4/NiFeOH-350	1 M KOH	197	-	94	S21
21	MoS_2/NiFe LDH	1 M KOH	98	-	95	S22

[a] η_{-10} is overpotential at a current density of -10 mA cm^{-2}; [b] η_{-50} is overpotential at a current density of -50 mA cm^{-2}.

Table S3. Comparison of cell potential for overall water splitting performance of the synthesized electrode materials with recently reported non-noble transition metal-based results.

Sl. No.	Electrolyzer	Electrolyte	$E_{cell}{}^{a)}$ (V) @ 10 mA cm^{-2}	References
1	$Co(OH)_2$@FeOOH/NF ‖ $Co(OH)_2$@FeOOH/NF	1 M KOH	1.58	This work
2	Co_3O_4@Fe_3O_4/NF ‖ Co_3O_4@Fe_3O_4/NF	1 M KOH	1.7	This work
3	Co_2P@Fe_2P/NF ‖ Co_2P@Fe_2P/NF	1 M KOH	1.53	This work
4	FeOOH/NF ‖ FeOOH/NF	1 M KOH	1.65	This work
5	$Co_{0.025}$-NiFe-LDH/NF ‖ $Co_{0.025}$-NiFe-LDH/NF	1 M KOH	1.58	S7
6	Co(OH)F@CoFe-LDH ‖ Co(OH)F@CoFe-LDH	1 M KOH	1.58	S8
7	Co3Fe7@NCNTFs ‖ Co3Fe7@NCNTFs	1 M KOH	1.64	S9
8	CoFeSP/CNT ‖ CoFeSP/CNT	1 M KOH	1.632	S10
9	$CoMoRuO_x$-350 ‖ Pt/C	1 M KOH	1.55	S11
10	Mo-CoP (1/2.3) ‖ Mo-CoP (1/2.3)	1 M KOH	1.7	S12
11	Co_3S_4@rGO ‖ Co_3S_4@rGO	0.5 M H_2SO_4	1.82	S14
12	FeCoNiP@NC ‖ FeCoNiP@NC	1 M KOH	1.73	S15
13	Co@BNPCFs-800 ‖ Co@BNPCFs-800	1 M KOH	1.596	S17

14	$Co/Mo_2C@C \| Co/Mo_2C@C$	1 M KOH	1.59	S18
15	Ni-Fe-S/Cu ‖ Ni-Fe-S/Cu	1 M KOH	1.705	S19
16	Co@NC nanocage/HCF_{200} ‖ Co@NC nanocage/HCF_{200}	1 M KOH	1.618	S20
17	Fe-Ni_5P_4/NiFeOH-350 ‖ Fe-Ni_5P_4/NiFeOH-350	1 M KOH	1.55	S21
18	MoS_2/NiFe LDH ‖ MoS_2/NiFe LDH	1 M KOH	1.61	S22
19	Co_3S_4@NiCo-LDH ‖ Co_3S_4@NiCo-LDH	1 M KOH	1.59	S23

a) E_{cell} is cell potential.

References

S1 G. Kresse and J. Furthmuller, *Comput. Mater. Sci.*, 1996, **6**, 15.

S2 G. Kresse and J. Furthmuller, *Phys. Rev. B*, 1996, **54**, 11169.

S3 J. P. Perdew, K. Burke and M. Ernzerhof, *Phys. Rev. Lett.*, 1996, **77**, 3865.

S4 G. Kresse and D. Joubert, *Phys. Rev. B*, 1999, **59**, 1758.

S5 S. Grimme, J. Antony, S. Ehrlich, H. Krieg, *J. Chem. Phys.*, 2010, **132**, 154104.

S6 G. Rajeshkhanna, S. Kandula, K. R. Shrestha, N. H. Kim and J. H. Lee, *Small*, 2018, **14**, 1803638.

S7 Y. Liu, S. He, Y. Chen, Z. Zou and Q. Wang, *J. of Power Sources*, 2021, **506**, 230097.

S8 M. Qin, Y. Wang, H. Zhang, M. Humayun, X. Xu, Y. Fu, M. K. Kadirov and C. Wang, *CrystEngComm*, 2022, **24**, 6018-6030.

S9 Q. Yuan, Y. Yu, P. C. Sherrell, J. Chen and X. Bi, *Chem. Asian J.*, 2020, **15**, 1728-1735.

S10 L. Huang, H. Wu, H. Liu and Y. Zhang, *Electrochim. Acta*, 2019, **318**, 892-900.

S11 C. Wang, H. Shang, Y. Wang, H. Xu, J. Li and Y. Du, *J. Mater. Chem. A*, 2021, **9**, 14601-14606.

S12 L. Li, Y. Guo, X. Wang, X. Liu and Y. Lu, *Langmuir*, 2021, **37**, 5986-5992.

S13 A. Muthurasu, G. P. Ojha, M. Lee and H. Y. Kim, *Electrochim. Acta*, 2020, **334**, 135537.

S14 R. S. Kumar, S. C. Karthikeyan, S. Ramakrishnan, S. Vijayapradeep, A. R. Kim, J. S. Kim and D. J. Yo, *Chem. Eng. J.*, 2023, **451**, 138471.

S15 J. Sun, S. Li, Q. Zhang and J. Guan, *Sustainable Energy Fuels*, 2020, **4**, 4531-4537.

S16 P. Zhang, X. F. Lu, J. Nai, S. Q. Zang and X. W. Lou, *Adv. Sci.*, 2019, **6**, 1900576.

S17 F. Guo, Z. Liu, J. Xiao, X. Zeng, C. Zhang, Y. Lin, P. Dong, T. Liu, Y. Zhang and M. Li, *Chem. Eng. J.*, 2022, **446**, 137111.

S18 S. Yuan, M. Xia, Z. Liu, K. Wang, L. Xiang, G. Huang, J. Zhang and N. Li, *Chem. Eng. J.*, 2022, **430**, 132697.

S19 W. Xu, S. Zhao, J. P. Zhang, X. Yang, Y. X. Tang, Y. W. Han and Y. Shen, *Int. J. Hydrog. Energy*, 2023, **48**, 18315-18325.

S20 R. Zhu, X. Yu, W. Li, M. Li, X. Bo and G. Gan, *J. Alloys Compd.*, 2023, **947**, 169488.

S21 C. F. Li, J. W. Zhao, L. J. Xie, J. Q. Wu and G. R. Li, *Appl. Catal. B: Environ.*, 2021, **291**, 119987.

S22 X. P. Li, L.R.Zheng, S. J. Liu, T. Ouyang, S. Ye and Z. Q. Liu, *Chin. Chem. Lett.*, 2022, **33**, 4761-4765.

S23 X. Xu, L. Su, Y. Zhang, L. Dong and X. Miao, *New J. Chem.*, 2021, **45**, 15429-15436.